

Journal of Biomedical Optics

SPIEDigitalLibrary.org/jbo

Application of Raman spectroscopy for visualizing biochemical changes during peripheral nerve injury *in vitro* and *in vivo*

Shinsuke Morisaki
Chikashi Ota
Ken-ichi Matsuda
Natsuko Kaku
Hiroyoshi Fujiwara
Ryo Oda
Hidenobu Ishibashi
Toshikazu Kubo
Mitsuhiro Kawata

Application of Raman spectroscopy for visualizing biochemical changes during peripheral nerve injury *in vitro* and *in vivo*

Shinsuke Morisaki,^a Chikashi Ota,^b Ken-ichi Matsuda,^c Natsuko Kaku,^b Hiroyoshi Fujiwara,^a Ryo Oda,^a Hidenobu Ishibashi,^a Toshikazu Kubo,^a and Mitsuhiro Kawata^c

^aKyoto Prefectural University of Medicine, Graduate School of Medical Science, Department of Orthopaedics, Kawaramachi Hirokoji, Kamigyo-ku, Kyoto 602-8566, Japan

^bAnalytical Application Center, Horiba, Ltd., Miyanohigashi, Kisshoin, Minami-ku, Kyoto 601-8510, Japan

^cKyoto Prefectural University of Medicine, Graduate School of Medical Science, Department of Anatomy and Neurobiology, Kyoto 602-8566, Japan

Abstract. Raman spectroscopy can be used for analysis of objects by detecting the vibrational spectrum using label-free methods. This imaging method was applied to analysis of peripheral nerve regeneration by examining the sciatic nerve *in vitro* and *in vivo*. Raman spectra of intact nerve tissue had three particularly important peaks in the range 2800–3000 cm⁻¹. Spectra of injured sciatic nerves showed significant changes in the ratio of these peaks. Analysis of cellular spectra suggested that the spectrum for sciatic nerve tissue reflects the axon and myelin components of this tissue. Immunohistochemical analysis showed that the number of axons and the myelinated area were reduced at 7 days after injury and then increased by 28 days. The relative change in the axon to myelin ratio showed a similar initial increase, followed by a decrease at 28 days after injury. These changes correlated with the band intensity ratio and the changes in distribution of axon and myelin in Raman spectral analysis. Thus, our results suggest that label-free biochemical imaging with Raman spectroscopy can be used to detect turnover of axon and myelin in peripheral nerve regeneration. © The Authors. Published by SPIE under a Creative Commons Attribution 3.0 Unported License. Distribution or reproduction of this work in whole or in part requires full attribution of the original publication, including its DOI. [DOI: [10.1117/1.JBO.18.11.116011](https://doi.org/10.1117/1.JBO.18.11.116011)]

Keywords: peripheral nerve regeneration; Raman spectroscopy; myelination.

Paper 130576RR received Aug. 10, 2013; revised manuscript received Oct. 18, 2013; accepted for publication Oct. 25, 2013; published online Nov. 26, 2013.

1 Introduction

Raman spectroscopy provides specific vibrational signatures of chemical bonds, allowing identification of molecules without labeling.¹ Raman spectra exhibit sharp spectral features based on molecular structures and tissue alignments,² which makes this spectroscopy useful for biomedical applications such as quantitative histochemical analysis of atherosclerosis, disease diagnosis, and physiological analysis of hemoglobin oxygen saturation.^{3–6}

Peripheral nerve injury occurs in conditions such as trauma, inflammation, and peripheral neuropathies.^{7,8} The peripheral nervous system has great potential for regeneration compared with the central nervous system, but appropriate treatment for peripheral nerve injury requires an accurate diagnosis with regard to the location of the lesion and the degree of injury. Current diagnostic approaches using electromyography⁹ and magnetic resonance imaging cannot detect the degree of injury or the rate of nerve regeneration.¹⁰ Experimental detection of peripheral nerve regeneration using immunohistochemical staining with specific antibodies for peripheral nerve tissue^{11,12} and behavioral studies also have limitations in terms of clinical diagnosis.¹³ Therefore, improvement of noninvasive methods is required for the evaluation of degeneration and regeneration of peripheral nerve tissue.

To address this challenge, intact and injured rat sciatic nerve were examined by Raman spectroscopy including the peripheral nerve tissue and cells in this tissue. Changes in Raman spectra were compared with the morphological changes identified using immunohistochemical analysis. The results show that Raman spectroscopy is effective for chemical label-free diagnostic imaging of peripheral nerve regeneration.

2 Materials and Methods

2.1 Tissue Sample Preparation and Crush Injury

For tissue sample preparation, 6-week old Sprague–Dawley rats (Shimizu Laboratory Supplies, Kyoto, Japan) were used. The animals were maintained on a 12-h light/dark schedule with free access to food and water. The Committee for Animal Research, Kyoto Prefectural University of Medicine approved all surgical and experimental procedures. All surgical and experimental procedures were carried out in accordance with the guidelines of the National Institutes of Health on Animal Care.

All rats were deeply anesthetized using a mixture of oxygen and 2.0% isoflurane (Abbott Japan Co., Osaka, Japan). The right sciatic nerve was exposed and ligated at the proximal-thigh level using 3–0 silk to create a crush injury. Following ligation for 5 min, the suture was carefully released to produce a regenerating axonotmesis model.^{14,15} Samples were collected in the intact condition (day 0) at 7, 14, 21, and 28 days after crush injury ($n = 3$ for each time point).

Address all correspondence to: Hiroyoshi Fujiwara, Kyoto Prefectural University of Medicine, Graduate School of Medical Science, Department of Orthopaedics, Kawaramachi Hirokoji, Kamigyo-ku, Kyoto 602-8566, Japan. Tel: +81-75-251-5549; Fax: +81-75-251-5841; E-mail: fjwr@koto.kpu-m.ac.jp

For analysis of sciatic nerve tissue, the animals were deeply anesthetized and transcardially perfused with 0.9% NaCl, followed by 4% paraformaldehyde in 0.1 M phosphate-buffered saline (pH 7.4). After postfixation with 25% sucrose and cryoprotection, 15-mm segments of nerve tissue were sectioned by cryostat (14 μm ; CM3050S; Leica, Nussloch, Germany), including regions proximal and distal to the injury site in the longitudinal plane. The frozen sections were then mounted on the glass slides.

2.2 Raman Spectroscopy

Raman spectra were measured using a LabRam Aramis instrument (Horiba Jobin-Yvon, Kyoto, Japan) with a focal length of 460 mm and the entrance slit of the spectrometer set to 100 μm . The dispersive element had a grating of 600 lines/mm and spectral resolution was $<3\text{ cm}^{-1}$. Raman spectra were produced by excitation with a 532-nm laser focused on the sample through 50 \times and 100 \times microscope objectives (NA 0.75 and NA 0.9; Olympus, Japan). The lateral (x - y) spatial resolution was 2 μm and the depth (z) spatial resolution was 4 μm using the 50 \times objective lens. The lateral spatial resolution was 1 μm and the depth spatial resolution was 2 μm using the 100 \times objective lens. The objectives provided a laser spot of 1–2 μm on the sample. Laser power was set at 6.0 and 0.6 mW for analysis of sciatic nerve tissue and cells, respectively. Raman scattered light was collected in 180 deg back-scattering mode and recorded on a liquid nitrogen-cooled charge-coupled device camera (Symphony CCD detector; Horiba Scientific, Japan).

The serial mapping technique was used for the analysis of Raman nerve tissue spectra. Nerve tissue was placed on an automated motorized X , Y mapping stage and spectra were obtained at different points on the tissue by moving it under the microscopic objective. For mapping in the X , Y planes at chosen spatial resolutions, the sample was moved in both spatial dimensions (X and Y) and a spectrum was recorded at each (X , Y) position.¹⁶ The measured area of sciatic nerve tissue was $140 \times 140\ \mu\text{m}$, with a 10- μm step size in both dimensions.

To evaluate the peak changes quantitatively, three fields in each sample were randomly detected ($n = 9$ for each time points). The area of the C–H stretching band between 2770 and 3200 cm^{-1} was analyzed using a Gaussian Lorentzian fit with the center wavenumbers of the six components at 2853, 2890, 2940, 2976, 3010, and 3062 cm^{-1} . The ratio of band intensity (I2940/I2853) was calculated, in which the intensity at 2940 cm^{-1} was divided by that at 2853 cm^{-1} .

2.3 Distribution Analysis of Raman Spectra

To identify the components that contribute to the spectrum of intact sciatic nerve tissue, the classical least squares (CLS) method in LabSpec5 software (Horiba Jobin-Yvon)^{17,18} was used. This method is generally used for analysis of the components in a substance.¹⁹ In the current analysis, spectra of neurites of DRG and sphingomyelin were used as representative of axons and myelin, respectively. These spectra were summed and compared with the original spectrum of the intact sciatic nerve. To visualize the distribution of axons and myelin in sciatic nerve tissue, color images were constructed using mapping data for the intact sciatic nerve. The distribution of axon and myelin components at each mapping point of the sciatic nerve was expressed in separate spectra and a merged image was calculated. In the separate spectra, the greater the contribution to

the mapping point, the denser the color. Residual components (excluding axons and myelin) were also determined, with the color density expressing the intensity of these components in the tissue. The residual components were within 4.5% of the total intensity, which was regarded as an acceptable error.

Changes in the distributions of axon and myelin were also measured. The mapping data at each time point after crush injury were collected. The contributions of axon and myelin were obtained by dividing the mean density of each component by that of the total area in each mapping image and expressed as $C(\text{axon})$ and $C(\text{myelin})$. The axon/myelin ratio was calculated by dividing $C(\text{axon})$ by $C(\text{myelin})$. Before the application of chemometric method, spectra were baseline-corrected using piecewise linear correction with the same baseline points for all maps and reference spectra.

2.4 Primary Culture of Dorsal Root Ganglion Neurons and Schwann Cells

Dorsal root ganglion neurons (DRGs) were dissected from spinal cords of embryonic day 13.5 mice (Shimizu Laboratory Supplies) and treated with trypsin for 20 min in Hanks' buffered salt solution. Cells were dissociated mechanically and the trypsin reaction was terminated by the addition of Neurobasal medium (Gibco, Carlsbad, California). After centrifugation, cells were resuspended in DRG medium [Neurobasal medium (Gibco), penicillin/streptomycin (Gibco), 2% B27 (Gibco), 0.4% glucose, 2 mM L-glutamine, and 100 ng/ml nerve growth factor (Sigma–Aldrich, St. Louis, Missouri)] and plated on dishes coated with Matrigel (BD Biosciences, San Jose, California). Mitosis of non-neuronal cells was inhibited by 4-day treatment with 13 mg/ml 5-fluoro-2'-deoxyuridine initiated 24 h after plating. These cultures can be maintained indefinitely with half-volume changes of medium every 3 days. Primary cultures of Schwann cells were obtained from the sciatic nerve of P2 rats and plated onto 60-mm tissue culture dishes. The resulting cultures were maintained at 5% CO_2 at 37°C in Dulbecco's modified Eagle's medium containing 10% fetal bovine serum. To analyze phospholipids incorporated in myelin, we detected the presence of sphingomyelin using a Phospholipid kit (Avanti Polar Lipids, Inc. Alabaster, Alabama).²⁰

2.5 Immunocytochemistry

Cultured DRGs and Schwann cells were incubated overnight at 4°C with primary antibodies: mouse monoclonal antibody against Neurofilament 200 (Sigma–Aldrich) and mouse monoclonal antibody S100 (1:200; Abcam, Cambridge, Massachusetts). After rinsing off primary antibodies, the cells were incubated for 2 h at room temperature with a secondary antibody for staining (goat anti-mouse IgG labeled with Alexa 488; Molecular Probes, Eugene, Oregon) diluted 1:1000. The slides were then coverslipped with Gelvatol (20% polyvinyl alcohol and glycerol mixture) and imaged on a confocal laser-scanning microscope (Fluoview 300; Olympus). The detailed procedures for immunohistochemistry are described elsewhere.^{11,15}

2.6 Immunohistochemistry

Mounted sections were incubated overnight at 4°C with primary antibodies: rat monoclonal antibody against myelin basic protein (MBP; 1:2000; Millipore, Temecula, California) and rabbit

monoclonal antibody against NF200 (Sigma–Aldrich). After rinsing off primary antibodies, the sections were incubated for 2 h at room temperature with secondary antibodies for double staining (goat anti-rabbit IgG labeled with Alexa 488 and goat anti-rat IgG labeled with Alexa 548; both Molecular Probes) diluted 1:1000. Slides were analyzed with the procedure used for immunocytochemistry. In semiquantitative analysis of axonal and myelin changes, microscopic fields in each sample were randomly selected. Images were digitized on a gray scale using an automatic threshold tool linked to morphometry software (ImageJ, National Institutes of Health, Bethesda, Maryland). The mean number of axons was counted in the field (area: $1.25 \times 10^2 \text{ mm}^2$) and expressed as the number per mm^2 (N/mm^2). The myelinated area was expressed as the MBP-immunopositive area divided by the total area (%). To evaluate the relative changes of axon to myelin, the number of axons was divided by the myelinated area and expressed as the axon/myelin ratio.

2.7 Statistical Analysis

All results are expressed as means \pm standard deviation. Nonparametric one-way analysis of variance was used within the same group to evaluate the significance of differences at multiple time points, with a Tukey-Kramer post hoc test. All statistical analyses were performed using JMP6 software (SAS Institute, Cary, North Carolina).

3 Results

3.1 Raman Spectra of Intact and Injured Sciatic Nerves

Raman spectra of an intact rat sciatic nerve tissue were examined. An epi-illumination image of longitudinally sectioned intact sciatic nerve segments is shown in Fig. 1(a). Raman mapping of the rectangular region of Fig. 1(a) at $1\text{-}\mu\text{m}$ intervals gave the mean spectrum shown in Fig. 1(b). Prominent peaks in the range were 1091, 1302, 1450, 1660, 2853, 2885, and 2940 cm^{-1} . The Raman bands at 1091, 1302, 1450, and 1660 cm^{-1} correspond to C–C stretching vibration, amide III, CH deformation, and amide I, respectively (Table 1).^{21,22} These bands are mainly derived from the lipid and protein contents. The bands at 2853 and 2885 cm^{-1} arise from symmetric and asymmetric CH_2 stretching modes. The CH_2 vibration modes mainly reflect lipid contents. The band at 2940 cm^{-1} is assigned to CH_3 symmetric stretching, which is derived from methyl groups that are abundant in proteins.

To examine changes in Raman bands in injured sciatic nerve compared with the intact sciatic nerve, spectra were collected at 7, 14, 21, and 28 days after crush injury. The mapping area was collected from a 5-mm portion distal to the crush site [Fig. 1(c)]. The three peaks from 2800 to 3000 cm^{-1} exhibited clear post-injury changes. Changes were not observed in the region at $1000\text{--}1800 \text{ cm}^{-1}$, which reflects chemical structures including amides I and III. Therefore, we focused on the range

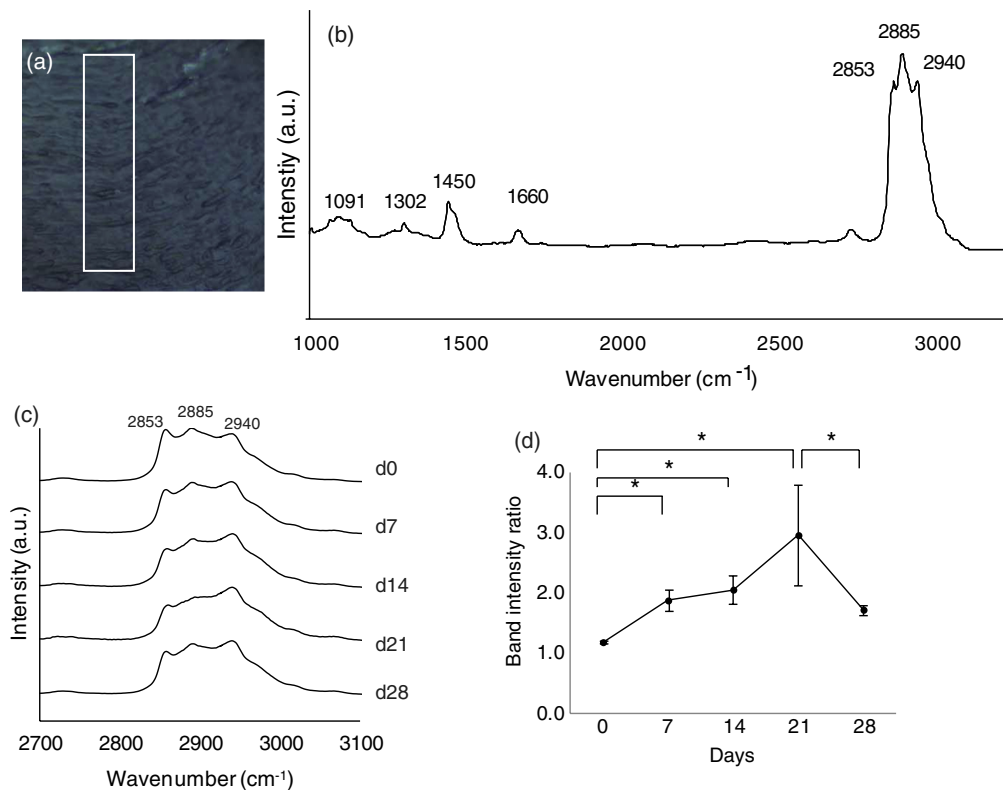


Fig. 1 Raman spectra of sciatic nerve tissue. (a) Epi-illumination image of Raman spectra in longitudinally sectioned sciatic nerve segments. (b) Mean spectrum collected from the Raman mapping of intact sciatic nerve in the rectangular region of a. Prominent Raman peaks are at 1091, 1302, 1450, 1660, 2853, 2885, and 2940 cm^{-1} . (c) Time-dependent Raman spectra of injured sciatic nerve in the range $2800\text{--}3000 \text{ cm}^{-1}$ at 0, 7, 14, 21, and 28 days after crush injury. The peak at 2853 cm^{-1} showed a decrease after injury and the peak at 2940 cm^{-1} had a relative increase. (d) Quantitative analyses of the band intensity ratio (I_{2940}/I_{2853}) for each time point. The ratio increased at 21 days after injury, but then decreased at 28 days. Values are expressed as means \pm standard deviation. *Significant difference between time points ($P < 0.05$).

Table 1 Representative Raman spectra collected from sciatic nerve tissue and the chemical bond corresponding to each Raman band.

Wavenumber (cm ⁻¹)	Chemical bonds
1091	C–C stretching (lipid and protein)
1302	Amide III (protein contribution of axon), in-plane CH ₂ twist from lipid
1440–1470	C–H deformation arising from CH ₂ and CH ₃ of lipid and protein
1663	Amide I (protein contribution of axon), C=C from lipid
1740	C=O band (mainly from lipid)
2850	CH ₂ symmetric (mainly from lipid)
2885	CH ₂ asymmetric (mainly from lipid)
2940	CH ₃ symmetric (mainly from protein)

2800–3000 cm⁻¹. The peak at 2853 cm⁻¹ showed a decrease after injury and that at 2940 cm⁻¹ showed a relative increase. At 28 days after injury, the peak at 2940 cm⁻¹ showed an apparent decrease compared with that at 2885 cm⁻¹.

To evaluate these peak changes quantitatively, the band intensity ratio (I₂₉₄₀/I₂₈₅₃) was calculated [Fig. 1(d)]. This ratio showed a significant increase after injury that continued for 21 days. At 28 days after injury, the ratio decreased significantly.

3.2 Raman Spectra of Cultured DRG Neurons and Schwann Cells

Transmission images of DRG neurons and Schwann cells [Figs. 2(a) and 2(c)] and immunofluorescent images [Figs. 2(b) and 2(d)] of these cells were obtained after collection of Raman spectra [Fig. 2(e)]. In these spectra of neurites of DRGs, a prominent peak was located at 2940 cm⁻¹, which is due to CH₃ symmetric stretching. Prominent peaks for Schwann cells occurred at 2851, 2885, and 2909 cm⁻¹, which are associated with CH₂ vibration modes reflecting lipid contents. The peak pattern of axons was distinct from that of Schwann cells in the 2800–3000 cm⁻¹ range. The Raman spectra of pure sphingomyelin, one of the main phospholipids in myelin, also showed prominent peaks at 2800–3000 cm⁻¹, similar to those for Schwann cells. This finding suggests that the peaks observed for Schwann cells reflect the composition of myelin.

3.3 Distribution Analysis of Raman Spectra

To compare Raman bands of cells with those of sciatic nerve tissue, we focused on the CH stretching bands in the 2800–3000 cm⁻¹ range. In this region, neurites of DRGs showed a prominent peak at 2940 cm⁻¹ [Fig. 3(a)], while peaks for sphingomyelin were found at 2853 and 2885 cm⁻¹ [Fig. 3(b)]. The neurites of DRGs and sphingomyelin are representative of the axon and myelin components, respectively. To analyze how each component contributes to the spectrum of intact sciatic nerve tissue, spectra of neurites of DRGs and sphingomyelin

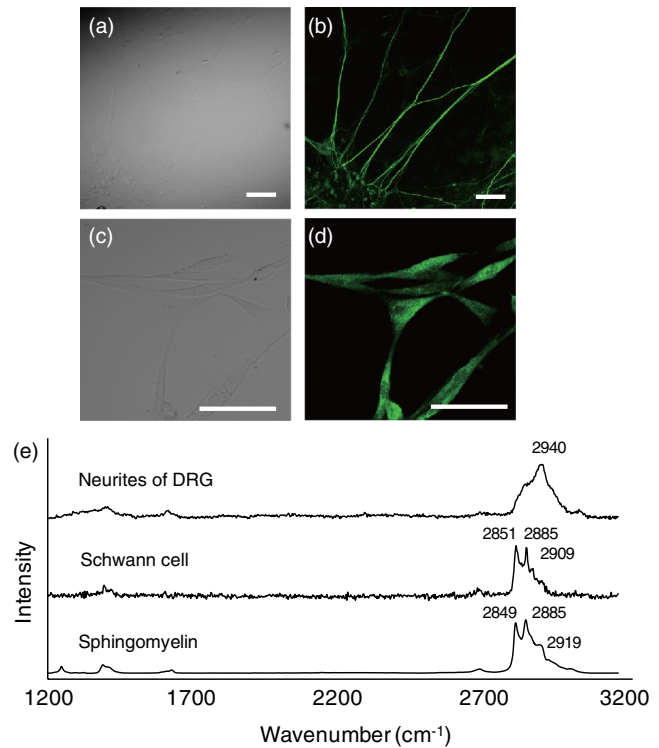


Fig. 2 Raman spectra of cultured DRG neurons and Schwann cells. Transmission images (a and c) and immunofluorescent images (b and d) of DRG neurons (a and b) and Schwann cells (c and d). Scale bars = 50 μm. (e) Raman spectra of neurites of a DRG neuron and cell bodies of Schwann cells. Prominent Raman peaks of neurites are at 2886 and 2940 cm⁻¹. Raman Schwann cell peaks are at 2851, 2885, and 2909 cm⁻¹. Raman spectra of sphingomyelin were also detected, in which Raman peaks are at 2849, 2885, and 2919 cm⁻¹. The Schwann cell Raman spectrum between 2800 and 3000 cm⁻¹ showed a similar pattern to that of sphingomyelin.

were summed using the CLS method. The summed spectra [shown in black in Fig. 3(c)] was similar to the spectrum for intact sciatic nerve tissue [shown in red in Fig. 3(c)].

To investigate how axons and myelin were distributed in sciatic nerve tissue, color images were constructed using mapping data for intact sciatic nerves. With reference to the spectra in Figs. 3(a) and 3(b), the distributions of axon and myelin components at each mapping point of the sciatic nerve are shown in green [Fig. 3(d)] and red [Fig. 3(e)], respectively. The merged image is shown in Fig. 3(f). The green and red areas are aligned in parallel, similar to the typical structure of peripheral nerves in longitudinal slices [Figs. 4(a)–4(c)]. The image of the residual components is shown in Fig. 3(g).

To examine how the distribution of axons and myelin changes in injured sciatic nerve, the ratio of the contributions of axon and myelin was calculated [Fig. 3(h)]. The results showed an initial trend for an increase followed by a reduction at 28 days after injury, similar to the changes in the band intensity ratio.

3.4 Immunohistochemical Analysis in Intact and Crush-Injured Sciatic Nerves

For comparison with the Raman spectral changes, we performed immunohistochemical analysis using the serial sections used in the Raman spectroscopic analysis [Figs. 4(a)–4(o)]. In intact sciatic nerve (d0), axons staining positively for NF200 [Fig. 4(a)]

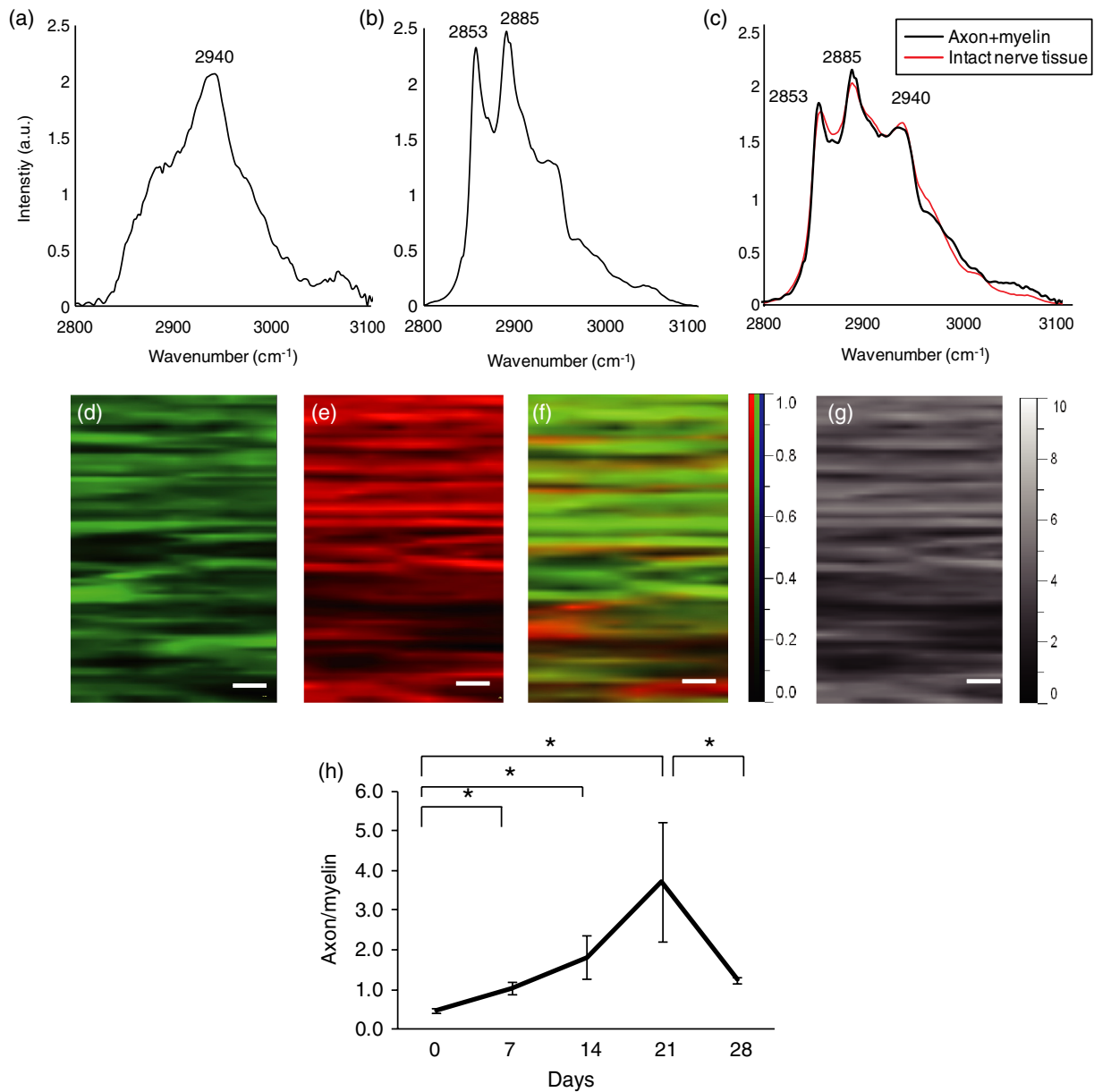


Fig. 3 (a–c) Spectra of intact sciatic nerve tissue shown in Fig. 1(b) were separated into two spectra, based on spectra for DRG neurites (a) and sphingomyelin (b). A summed spectrum of DRG neurites and sphingomyelin is shown in black (c). The spectra of intact sciatic nerve are shown in red (c). The summed spectrum and the spectrum for nerve tissue have similar patterns. (d–f) The distribution of axon (represented by DRG neuritis) and myelin components (represented by sphingomyelin) in intact sciatic nerve tissue is expressed in colored images: axons in green (d), myelin in red (e), and a merged image (f). These figures show that myelin was aligned parallel to axons. (g) Residual component image. (h) Time-dependent changes in the distribution ratio of axons divided by myelin in injured sciatic nerve. The changes in the distribution of axon and myelin were similar to the band intensity ratios.

and myelin staining positively for MBP [Fig. 4(b)] are aligned in parallel, reflecting the typical structure in which myelin wraps around the axon. After crush injury, immunopositive axons and myelin decreased because of Wallerian degeneration. At 14 days after injury, immunopositive nerve fibers were observed. The increase in regenerated axons and myelin with the restructuring of peripheral nerve tissue was confirmed at 28 days after injury. Quantitative analysis showed that the number of axons and the myelinated area were significantly decreased at 7 days after crush injury, and then increased until 28 days after injury [Figs. 4(p) and 4(q)]. To analyze the relative change, the axon to myelin ratio was calculated. This ratio increased until 21 days

after injury and then showed a significant reduction at 28 days [Fig. 4(r)]. This change was correlated with the changes in the band intensity ratio [Fig. 1(d)] and distribution [Fig. 4(h)].

4 Discussion

In this study, we investigated whether a label-free method using Raman spectroscopy can be used to detect changes in peripheral nerve regeneration. This is the first study to examine peak patterns in Raman spectra in peripheral nerve regeneration *in vitro* and *in vivo*. The results showed that there are three strong peaks in the region 2800–3000 cm^{-1} in intact peripheral nerve tissue [Fig. 1(b)]. Spectra of injured sciatic nerves showed significant

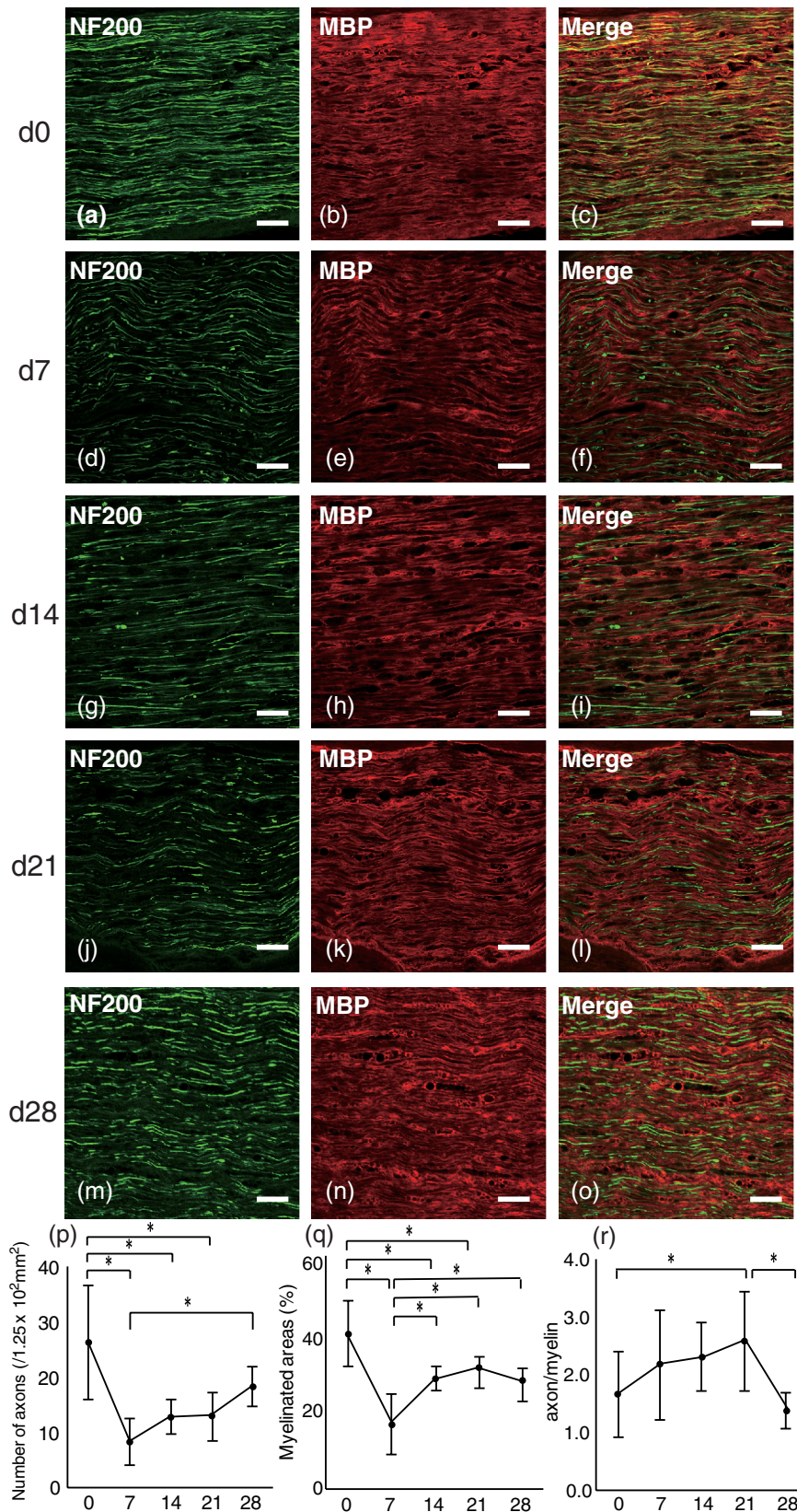


Fig. 4 Immunohistochemical analyses of serial sections of sciatic nerve. Axonal and myelin expressions are shown in injured sciatic nerves double-labeled with NF200 and MBP. Scale bars = 100 μm . Expression of NF200 (a, d, g, j, m), MBP (b, e, h, k, n), and merged images (c, f, i, l, o) in intact (a–c) and crush-injured sciatic nerves (d–o). The number of immunopositive axons (NF200) and myelin (MBP) are decreased at 7 days after injury. The immunoreactivity recovered by 14 days and gradually increased until 28 days. The number of axons (p) and the myelinated area (q) are shown. Relative axon and myelin changes are expressed as the axon/myelin ratio (r).

changes in the ratio of these peaks [Fig. 1(c)]. Analysis of cellular spectra suggested that the spectrum for sciatic nerve tissue reflects the axon and myelin components of this tissue (Figs. 2 and 3). Immunohistochemical results showed that the axon/myelin ratio initially increased after injury and then decreased at 28 days after injury [Fig. 4(r)]. Similar changes were seen in the band intensity ratio in the Raman spectra and in the axon/myelin distribution [Fig. 1(d)]. This correlation between Raman spectra and morphological changes suggests that Raman spectroscopy can be used as a label-free method to detect axon and myelin turnover during peripheral nerve injury.

Raman spectroscopy can detect the constituents of objects and has been used to detect abnormalities in biological tissue and cells.^{23–27} In the current study, Raman mapping data of peripheral nerve tissue in longitudinal sections of intact sciatic nerve tissue in the range 2800–3000 cm^{-1} showed three strong peaks at 2853, 2885 and 2940 cm^{-1} [Fig. 1(b)]. The bands at 2853 and 2885 cm^{-1} are derived from lipids,^{21,22} and peripheral nerve tissue is rich in lipids in myelin sheaths that surround axons to support neural electrical activity.^{28–31} Myelin is supplied by Schwann cells and myelin lipids include sphingomyelin and the glycolipid galactocerebroside. Schwann cells had similar spectral patterns at 2851 and 2885 cm^{-1} and Raman spectra of sphingomyelin showed similar patterns to that of Schwann cells. Therefore, the region at 2853 and 2885 cm^{-1} reflects the presence of lipids, including sphingomyelin.

Raman spectra of the intact sciatic nerve tissue also showed a strong peak at 2940 cm^{-1} [Fig. 1(b)]. This band is assigned to CH_3 symmetric stretching, reflecting the protein content of the tissue. Peripheral nerve tissue is a cord-like structure that contains many axons³² and neurofilament proteins are the most abundant fibrillar components of the axon cytoplasm.^{33–35} Neurofilaments are composed of polypeptide chains with long stretches of sequences rich in glutamic acid residues. Raman spectra of cultured DRG neurites also showed a single peak at 2940 cm^{-1} [Figs. 2(e) and 3(a)], which also corresponds to the results for nerve tissue. Therefore, the band at 2940 cm^{-1} reflects the protein contents, including those of axons. To examine the contribution of axon and myelin in intact sciatic nerves, a distribution analysis was performed. The summed spectrum of axon and myelin was similar to that of intact sciatic nerve tissue [Fig. 3(c)], indicating that the spectrum of the intact sciatic nerve largely reflects the axon and myelin constituents.

Injured nerves were examined to determine if Raman spectra can be used to detect chemical changes during peripheral nerve regeneration [Fig. 1(c)]. There was a significant increase in the band intensity ratio (I2940/I2853) until 21 days after crush injury, followed by a decrease at 28 days [Fig. 1(d)]. These results suggest volume changes in protein and lipid components derived from axon and myelin, respectively. To investigate the effect of constituents on the changes in the band intensity ratio, changes in the distribution of axons and myelin were analyzed [Fig. 3(h)]. The results showed a relative increase of axon to myelin up to 21 days after injury and a reduction at 28 days. The cause of the volume changes was examined in morphological analysis using markers for axons and myelin (Fig. 4). Both axons and myelin decreased at 7 days, and then gradually increased up to 28 days [Fig. 4(p)]. These changes are consistent with the typical changes during peripheral degeneration and regeneration. In Wallerian degeneration, proteins and lipids are both degraded in the distal portion of injured peripheral nerve tissue.³⁶ After Wallerian degeneration, the number of axons

increases and Schwann cells begin to remyelinate around axons, leading to an increase in protein content and lipid accumulation in peripheral nerve tissue. Although axon and myelin showed a similar pattern of regeneration, the rates of increase were different. Thus, the axon to myelin ratio increased up to 21 days and then showed a decrease at 28 days, with a correlation of the band intensity ratio and distribution changes [Fig. 4(r)]. Therefore, the Raman spectral changes in peripheral nerve regeneration reflected the compositional changes in protein and lipids, which were derived from the difference in regeneration rates of axons and myelin.

Several variations of Raman spectroscopy have been developed and some previous studies have examined Raman bands in peripheral nerve tissue.^{37–39} Coherent anti-Stokes Raman scattering (CARS) microscopy has been used to examine peripheral nerves based on structural changes in myelin, with the findings of demyelination up to 2 weeks after injury and remyelination at 3 weeks, showing that CARS can image peripheral nerves following demyelinating crush injury.³⁹ However, in standard CARS microscopy, only one type of vibration can be excited at one time.^{25,40} One advantage of Raman spectroscopy is that it is possible to collect detailed information over a wide spectrum without limiting the target wavelength, depending on the specific molecules under study.⁴¹ Our results revealed three peaks in the range 2800–3000 cm^{-1} and a significant change in the peak ratio in crush injury. Evaluation of the bands for axons and Schwann cells showed that the Raman peak changes in peripheral nerve degeneration and regeneration reflected compositional changes in axons and myelin.

5 Conclusions

This report shows that strong peaks for peripheral nerves in the region 2800–3000 cm^{-1} are obtained in Raman spectroscopy *in vitro* and *in vivo*, and that these peaks reflect changes in axons and myelin. We also found a correlation of the band intensity ratio and distribution changes with the immunohistochemical changes during peripheral nerve degeneration and regeneration. These findings suggest that the Raman spectroscopy is a useful tool for label-free detection of changes in axon and myelin turnover in peripheral nerve regeneration.

Acknowledgments

This work was supported by KAKENHI (24890199).

References

1. N. J. Crane and E. A. Elster, "Vibrational spectroscopy: a tool being developed for the noninvasive monitoring of wound healing," *J. Biomed. Opt.* **17**(1), 010902 (2012).
2. G. R. Holtom et al., "Achieving molecular selectivity in imaging using multiphoton Raman spectroscopy techniques," *Traffic* **2**(11), 781–788 (2001).
3. C. W. Freudiger et al., "Label-free biomedical imaging with high sensitivity by stimulated Raman scattering microscopy," *Science* **322**(5909), 1857–1861 (2008).
4. K. A. Esmonde-White et al., "Raman spectroscopy of synovial fluid as a tool for diagnosing osteoarthritis," *J. Biomed. Opt.* **14**(3), 034013 (2009).
5. C. Krafft et al., "Disease recognition by infrared and Raman spectroscopy," *J. Biophoton.* **2**(1–2), 13–28 (2009).
6. M. Ogawa et al., "Label-free biochemical imaging of heart tissue with high-speed spontaneous Raman microscopy," *Biochem. Biophys. Res. Commun.* **382**(2), 370–374 (2009).

7. J. Noble et al., "Analysis of upper and lower extremity peripheral nerve injuries in a population of patients with multiple injuries," *J. Trauma* **45**(1), 116–122 (1998).
8. J. A. Kouyoumdjian, "Peripheral nerve injuries: a retrospective survey of 456 cases," *Muscle Nerve* **34**(6), 785–788 (2006).
9. C. Marciniak et al., "Practice parameter: utility of electrodiagnostic techniques in evaluating patients with suspected peroneal neuropathy: an evidence-based review," *Muscle Nerve* **31**(4), 520–527 (2005).
10. S. Morisaki et al., "In vivo assessment of peripheral nerve regeneration by diffusion tensor imaging," *J. Magn. Reson. Imaging* **33**(3), 535–542 (2011).
11. M. Demestre et al., "Characterisation of matrix metalloproteinases and the effects of a broad-spectrum inhibitor (BB-1101) in peripheral nerve regeneration," *Neuroscience* **124**(4), 767–779 (2004).
12. V. T. Ribeiro-Resende et al., "Ganglioside 9-O-acetyl GD3 expression is upregulated in the regenerating peripheral nerve," *Neuroscience* **147**(1), 97–105 (2007).
13. J. R. Bain, S. E. Mackinnon, and D. A. Hunter, "Functional evaluation of complete sciatic, peroneal, and posterior tibial nerve lesions in the rat," *Plast. Reconstr. Surg.* **83**(1), 129–138 (1989).
14. A. Boivin et al., "Toll-like receptor signaling is critical for Wallerian degeneration and functional recovery after peripheral nerve injury," *J. Neurosci.* **27**(46), 12565–12576 (2007).
15. S. Morisaki et al., "Endogenous glucocorticoids improve myelination via Schwann cells after peripheral nerve injury: an *in vivo* study using a crush injury model," *Glia* **58**(8), 954–963 (2010).
16. D. F. Steele et al., "The potential use of Raman mapping to investigate in vitro deposition of combination pressurized metered-dose inhalers," *AAAPS J.* **6**(4), e32 (2004).
17. H. G. Schulze et al., "Artificial neural network and classical least-squares methods for neurotransmitter mixture analysis," *J. Neurosci. Methods* **56**(2), 155–167 (1995).
18. C. A. Owen et al., "In vitro toxicology evaluation of pharmaceuticals using Raman micro-spectroscopy," *J. Cell. Biochem.* **99**(1), 178–186 (2006).
19. T. Hasegawa, "Spectral simulation study on the influence of the principal component analysis step on principal component regression," *Appl. Spectrosc.* **60**(1), 95–98 (2006).
20. O. Jahn, S. Tenzer, and H. B. Werner, "Myelin proteomics: molecular anatomy of an insulating sheath," *Mol. Neurobiol.* **40**(1), 55–72 (2009).
21. L. Chrit et al., "In vivo chemical investigation of human skin using a confocal Raman fiber optic microprobe," *J. Biomed. Opt.* **10**(4), 044007 (2005).
22. R. Bohme et al., "Biochemical imaging below the diffraction limit—probing cellular membrane related structures by tip-enhanced Raman spectroscopy (TERS)," *J. Biophoton.* **3**(7), 455–461 (2010).
23. M. Gniadecka et al., "Melanoma diagnosis by Raman spectroscopy and neural networks: structure alterations in proteins and lipids in intact cancer tissue," *J. Invest. Dermatol.* **122**(2), 443–449 (2004).
24. K. Fujita and N. I. Smith, "Label-free molecular imaging of living cells," *Mol. Cells* **26**(6), 530–535 (2008).
25. A. Downes et al., "Raman spectroscopy and CARS microscopy of stem cells and their derivatives," *J. Raman Spectrosc.* **42**(10), 1864–1870 (2011).
26. V. V. Pully, A. T. M. Lenferink, and C. Otto, "Time-lapse Raman imaging of single live lymphocytes," *J. Raman Spectrosc.* **42**, 167–173 (2011).
27. C. K. Huang et al., "Disentangling dynamic changes of multiple cellular components during the yeast cell cycle by in vivo multivariate Raman imaging," *Anal. Chem.* **84**(13), 5661–5668 (2012).
28. R. Perrot et al., "Axonal neurofilaments control multiple fiber properties but do not influence structure or spacing of nodes of Ranvier," *J. Neurosci.* **27**(36), 9573–9584 (2007).
29. P. Kursula, "Structural properties of proteins specific to the myelin sheath," *Amino Acids* **34**(2), 175–185 (2008).
30. W. Baron and D. Hoekstra, "On the biogenesis of myelin membranes: sorting, trafficking and cell polarity," *FEBS Lett.* **584**(9), 1760–1770 (2010).
31. A. Jana and K. Pahan, "Sphingolipids in multiple sclerosis," *Neuromol. Med.* **12**(4), 351–361 (2010).
32. D. L. Sherman and P. J. Brophy, "Mechanisms of axon ensheathment and myelin growth," *Nat. Rev. Neurosci.* **6**(9), 683–690 (2005).
33. P. F. Roslansky et al., "Polypeptide composition of squid neurofilaments," *Proc. Natl. Acad. Sci. U. S. A.* **77**(1), 404–408 (1980).
34. N. Geisler et al., "Protein-chemical characterization of NF-H, the largest mammalian neurofilament component; intermediate filament-type sequences followed by a unique carboxy-terminal extension," *EMBO J.* **4**(1), 57–63 (1985).
35. R. Martin, "The structure of the neurofilament cytoskeleton in the squid giant axon and synapse," *J. Neurocytol.* **25**(9), 547–554 (1996).
36. A. D. Gaudet, P. G. Popovich, and M. S. Ramer, "Wallerian degeneration: gaining perspective on inflammatory events after peripheral nerve injury," *J. Neuroinflamm.* **8**, 110 (2011).
37. Y. Fu et al., "Coherent anti-Stokes Raman scattering imaging of myelin degradation reveals a calcium-dependent pathway in lyso-PtdCho-induced demyelination," *J. Neurosci. Res.* **85**(13), 2870–2881 (2007).
38. T. B. Huff and J. X. Cheng, "In vivo coherent anti-Stokes Raman scattering imaging of sciatic nerve tissue," *J. Microsc.* **225**(Pt 2), 175–182 (2007).
39. F. P. Henry et al., "Real-time in vivo assessment of the nerve micro-environment with coherent anti-Stokes Raman scattering microscopy," *Plast. Reconstr. Surg.* **123**(2 Suppl), 123S–130S (2009).
40. H. Wang et al., "Coherent anti-stokes Raman scattering imaging of axonal myelin in live spinal tissues," *Biophys. J.* **89**(1), 581–591 (2005).
41. G. J. Puppels et al., "Studying single living cells and chromosomes by confocal Raman microspectroscopy," *Nature* **347**(6290), 301–303 (1990).